Supporting Information

Gold Nanoparticle-Decorated Filter Papers as Hydrovoltaic Devices

Graham Beaton, Rahul Kumar, Nick Neokleous, Guojun Liu, and *Kevin Stamplecoskie

Queen's University Department of Chemistry, Chernoff Hall, 90 Bader Ln., Kingston, Ontario, CA

Contents

1. Instrumentation

1.1 Mass Balance Instrumentation

Mass data was acquired with a Mettler AT20 analytical balance. The uncertainty in this device is 0.1 mg, which is the smallest increment on the digital device.

1.2 UV-Vis Instrumentation

UV−Vis absorption spectra were acquired with a Varian Cary 60 UV-Vis spectrophotometer. Scanning from 300-900 nm.

1.3 SEM Instrumentation

Scanning Electron Microscopy was performed using a Thermo Fisher Quanta 250 SEM with Everhart-Thornley, Concentric Backscattered Electron, Large Field, and Gaseous Secondary Electron detector, acquired at various magnification

1.4 XRD Instrumentation

Acquisition of XRD spectra was done using a Bruker D2 Phaser diffractometer with Cu K_α radiation (1.54184 Å) over the 2θ range of 10−80°, with a step size of 0.002°.

XRD spectra were peak matched using FCC gold nanoparticles by reference (1).[1]

1.5 Potentiostat/Galvanostat Instrumentation

The Open Circuit Potential (OCP) and Linear Sweep Voltammetry (LSV) data was collected using the Autolab PGSTAT204 (compact and modular potentiostat/galvanostat) and NOVA 2.1 software.

2. Open Circuit Potential (OCP) and Linear Sweep Voltammetry (LSV) Triplicate Scans

2.1 OCP Scans
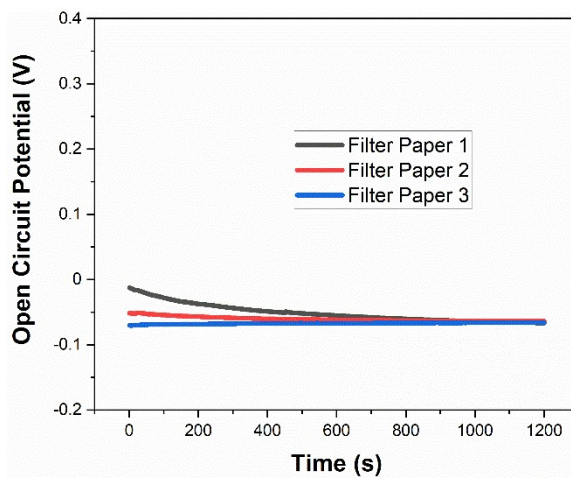
Figure S1. Measured Open Circuit Potential for three bare filter paper devices.
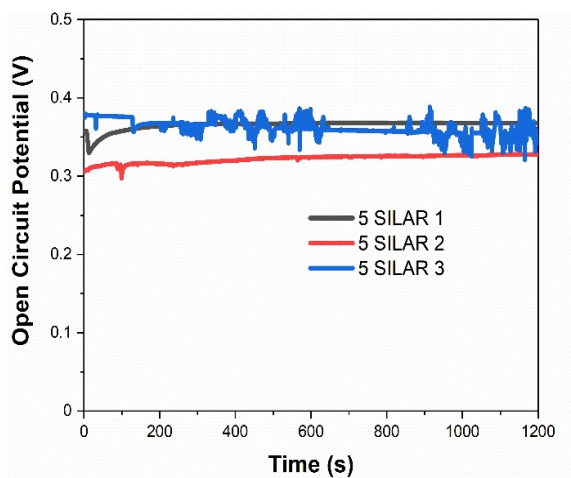
Figure S2. Measured Open Circuit Potential for three 5-SILAR devices.
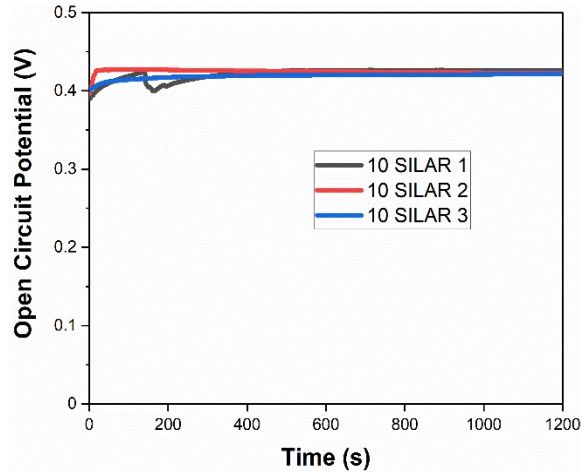
Figure S3. Measured Open Circuit Potential for three 10-SILAR devices.
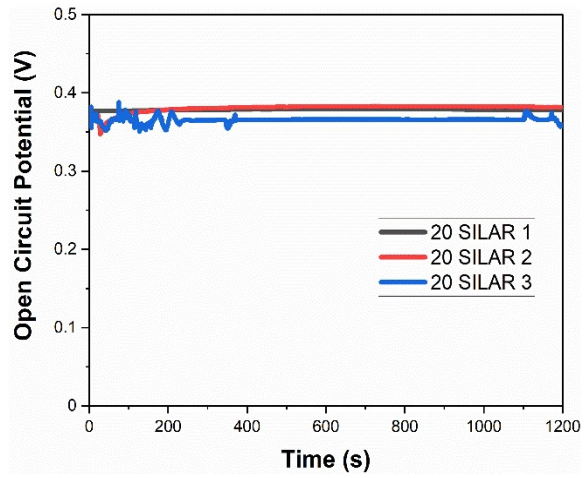
Figure S4. Measured Open Circuit Potential for three 20-SILAR devices.
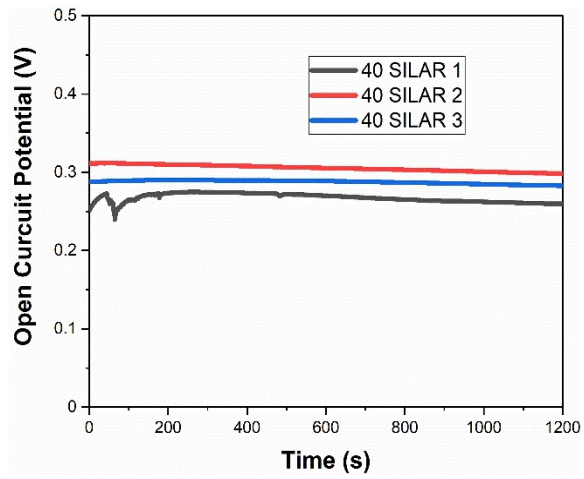
Figure S5. Measured Open Circuit Potential for three 40-SILAR devices.

2.1 LSV Scans
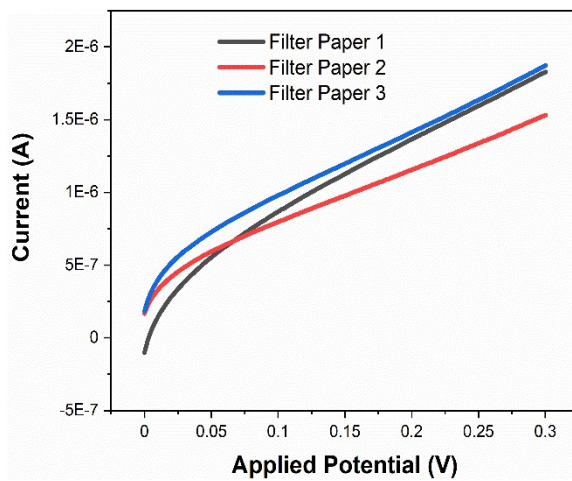
Figure S6. Short Circuit Current measured by LSV for the three bare filter paper devices.
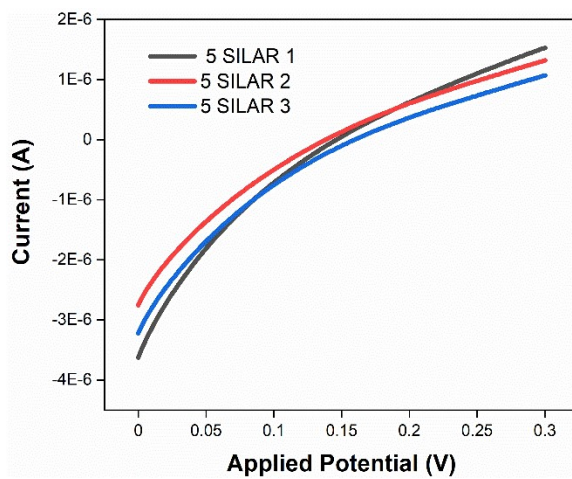
Figure S7. Supplementary LSV data for the three 5-SILAR devices.
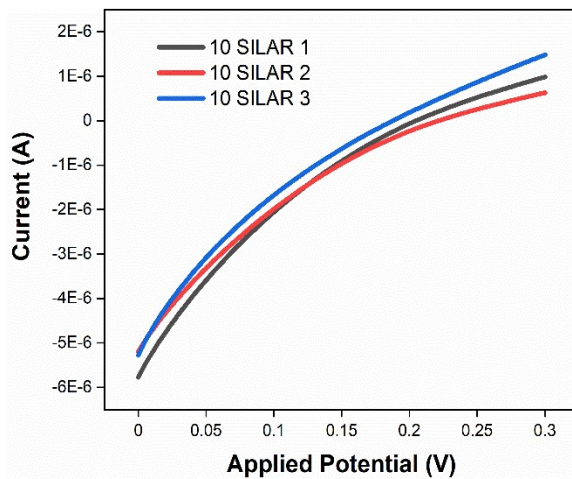
Figure S8. Supplementary LSV data for the three 10-SILAR devices.
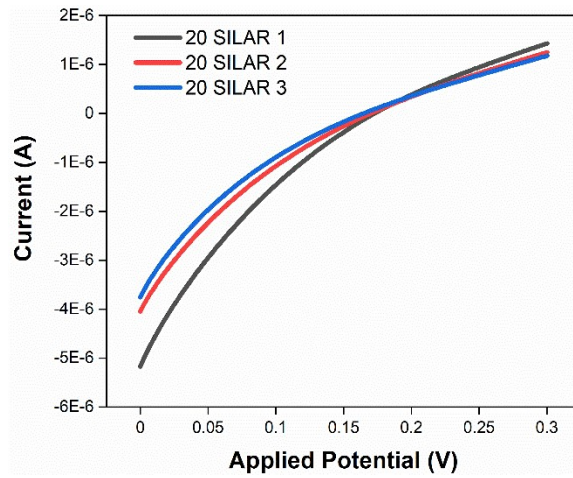
Figure S9. Short Circuit Current measured by LSV data for three 20-SILAR devices.
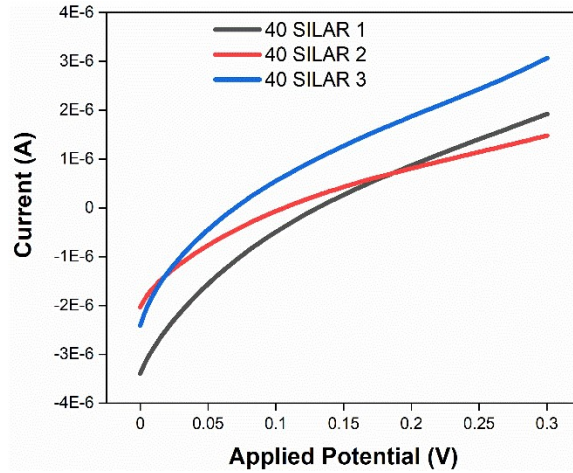
Figure S10. Short Circuit Current measured by LSV data for three 40-SILAR devices.

3. X-ray Diffraction (XRD) Results and Approximation of Gold Nanoparticle Diameter

3.1 XRD Results
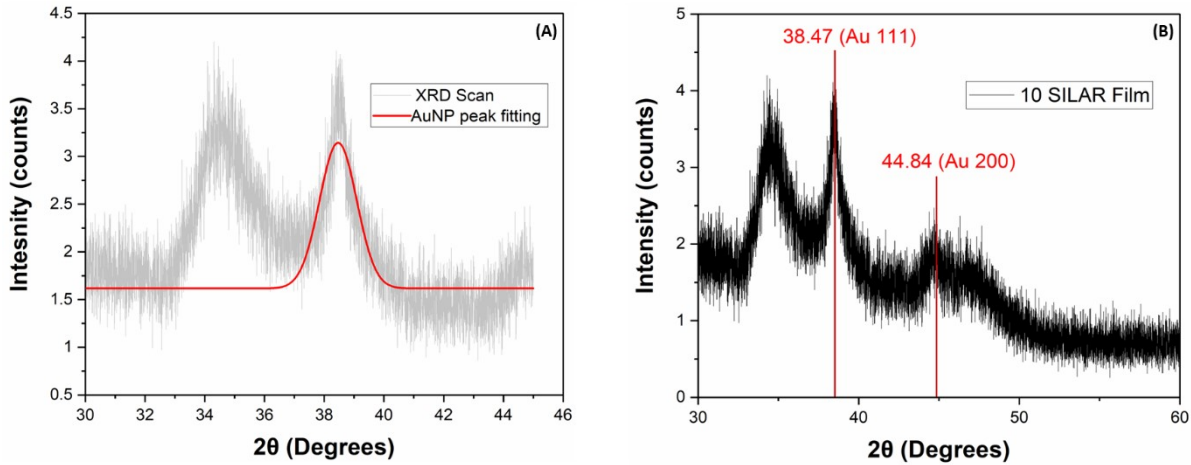
Figure S11. XRD scan of AuNP with peak fitting overlaid (A) and XRD scan and peak assignment for AuNP film (B).

3.2 Scherrer Equation

XRD is a useful technique for characterizing solid materials, providing information on crystalline structure, orientation, and other structural parameters.[2] It was used to confirm the presence of AuNP with a distinct peak visible for the 111 crystallographic face of face-centered cubic AuNP at approximately 38.47 (2θ Deg)[3, 4], or 0.671 radians. This peak is used to calculate particle size using the Scherrer (Equation 1)[3, 4]. This can be used to provide an approximation of the average diameter of the grown gold nanoparticles.

$$\tau = \frac{K\lambda}{\beta \cos\left(\frac{\theta}{2}\right)} \#(1)$$

Where: τ is the mean size of the ordered (crystalline) domains, K is a dimensionless shape factor, λ is the X-ray wavelength, β is the line broadening at the full width at half maximum (FWHM) intensity of the peak of interest, and θ is the Bragg angle.

For the face-centered cubic crystalline structure a dimensionless shape factor of 0.9 can be used.[5] The X-ray wavelength was 0.154 nm. The line broadening at the FWHM intensity, and Bragg Angle were found to be 0.0256 radians and 0.671 radians respectively. Based on these values, the mean diameter was calculated as follows:

$$\tau = \frac{0.9(0.154\ nm)}{0.0256\cos\left(\frac{0.671}{2}\right)} = 5.75\ nm$$

Resulting in an estimated diameter of 5.75 nm for the AuNP species functionalizing our devices.

3.3 Scherrer Equation Error Propagation

The error in the particle diameter can be calculated based on Equation 1, using the standard error propagation formula (Equation 2).

$$\delta t = |t| \sqrt{\left(\frac{\delta K}{K}\right)^2 + \left(\frac{\delta \lambda}{\lambda}\right)^2 + \left(\frac{\delta \beta}{\beta}\right)^2 + \left(\frac{\frac{\delta \theta}{2}\sin\left(\frac{\theta}{2}\right)}{\cos\left(\frac{\theta}{2}\right)}\right)^2} \quad \#(2)$$

Where δ denotes the uncertainty/error in each value. Since K, the dimensionless shape factor, is a constant, there is no error and as such $\delta K = 0$.

Furthermore, the wavelength bandwidth for the XRD instrumentation used could not be found, and as such it was treated as though there was no uncertainty in the wavelength, therefore $\delta \lambda = 0$.

The FWHM intensity (β) has a value of 0.0256 radians, and the standard error for this value ($\delta \beta$) was found to be 0.0003 radians. This represents the standard error as determined by Origin following the completion of 29 Gaussian peak fitting iterations.

Finally, the Bragg angle (θ) has a value of 0.671 radians. The instrumentation error is 0.02 degrees[6] or 0.0003 radians and the standard error, determined by Origin, is 0.0001 radians. The instrumentation and standard error were added together as follows to give the total Bragg angle errror:

$$\delta \theta = \sqrt{0.0003^2 + 0.0001^2} = 0.0004 \; radians$$

It should be additionally noted that since θ is contained in the cosine function, the error is not propagated as $(\delta\theta/\theta)^2$ as expected. Instead, the error is propagated as:

$$\cos\left(\frac{\delta \theta}{2}\right) = \frac{\delta \theta}{2}\sin\left(\frac{\theta}{2}\right)$$

Substituting all known values into Equation 2:

$$\delta t = |5.75 \; nm| \sqrt{\left(\frac{0.0003}{0.0256}\right)^2 + \left(\frac{\frac{0.0004}{2}\sin\left(\frac{0.671}{2}\right)}{\cos\left(\frac{0.671}{2}\right)}\right)^2} = \pm \; 0.07 \; nm$$

3.4 Additional SEM imaging
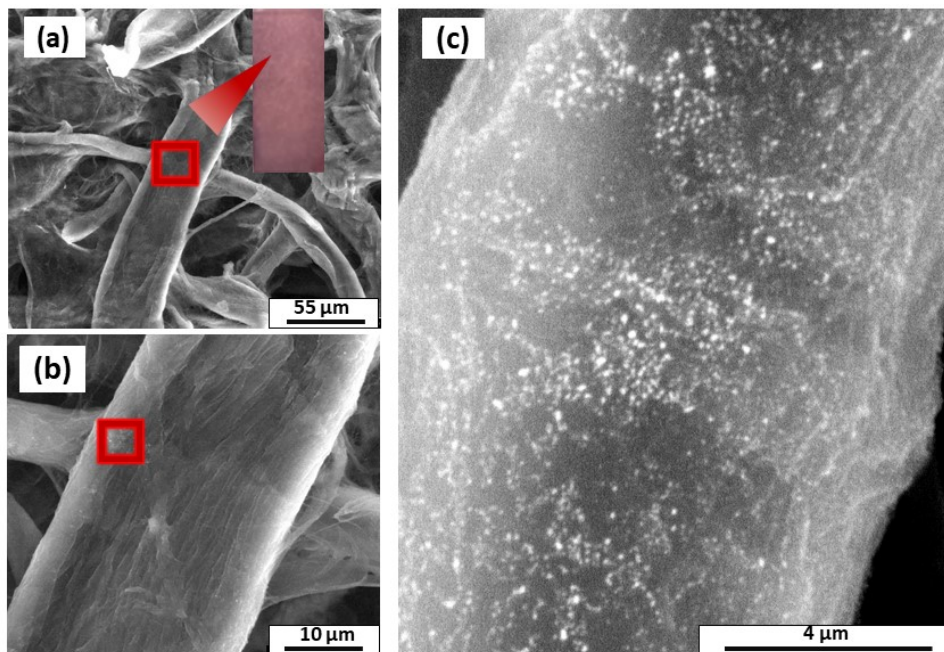
Figure S12: SEM images of a 10-SILAR gold decorated filter paper with increasing magnifications of 1X (an inset of a 10-SILAR device is also shown) (a), 5.5X (b), and 14X (c).

4. Power Output Density and Error Propagation

4.1 Ideal Power Output Density

The power density of the devices were calculated using the standard equation for power output density described Equation 3:

$$|Pd| = \left| \frac{V_{OC} I_{SC}}{M} \right| \quad \#(3)$$

Where: Pd is the power output density of the device, V_{OC} is the open circuit voltage, I_{SC} is the short circuit current, and M is the mass of the filter paper plus gold nanoparticles (i.e., the mass of the device).

This treatment was used for each device and a representative calculation for the best performing device (10-SILAR cycles) is shown below ($V_{OC} = 0.424$ V; $I_{SC} = -5.4$ uA; M = 48.90 mg):

$$|Pd| = \left| \frac{(0.424 V \times -5.4 \times 10^{-6} A)}{48.90 \times 10^{-3} g} \right| = 4.705 \times 10^{-5} \frac{W}{g} = 47.05 \frac{\mu W}{g}$$

4.2 Ideal Power Output Density Error Propagation

The error in power density for each device was calculated by propagating the standard deviation for each measurement using Equation 4:

$$\delta Pd = |Pd| \sqrt{\left(\frac{\delta V_{OC}}{V_{OC}} \right)^2 + \left(\frac{\delta I_{SC}}{I_{SC}} \right)^2 + \left(\frac{\delta M}{M} \right)^2} \quad \#(4)$$

Where: Pd is the power output density of the device, V_{OC} is the open circuit voltage of the device, I_{SC} is the short circuit current, and M is the mass. Furthermore, δPd, δV_{OC}, δI_{SC}, and δM denote the error in power output density, open circuit voltage, short circuit current, and mass respectively.

The error calculation remained the same for each device and so a representative calculation for the best performing device (10-SILAR cycles) is shown below:

$$\delta Pd = \left| 47.0 \frac{\mu W}{g} \right| \sqrt{\left(\frac{0.002\ V}{0.425\ V} \right)^2 + \left(\frac{0.3 \times 10^{-6} A}{-5.4 \times 10^{-6} A} \right)^2 + \left(\frac{0.4\ mg}{48.9\ mg} \right)^2} = \pm\ 2.74 \frac{\mu W}{g}$$

4.3 Power Output Density Under Load

To develop a better understanding of the actual device power output, a load study was carried out using a 1 kΩ, 10 kΩ, 100 kΩ, 1 MΩ, 4.5 MΩ, and 5.5 MΩ resistor. The maximum power output was found where the current and voltage intersected, which occurred at 0.17 MΩ. The current was 1.15 μA, with a voltage of 0.14 V. The device mass was 48.9 mg. Plugging known values into Equation 3:

$$|Pd| = \left| \frac{(0.14\ V \times 1.15 \times 10^{-6} A)}{48.90 \times 10^{-3} g} \right| = 3.29 \times 10^{-6} \frac{W}{g} = 3.3 \frac{\mu W}{g}$$

5. OCP and LSV Salt Comparison

To determine the optimal salt concentration, the OCP and LSV for a 10-SILAR device was tested at various salt concentrations. The results of this study are shown in Figures S12 and S13.
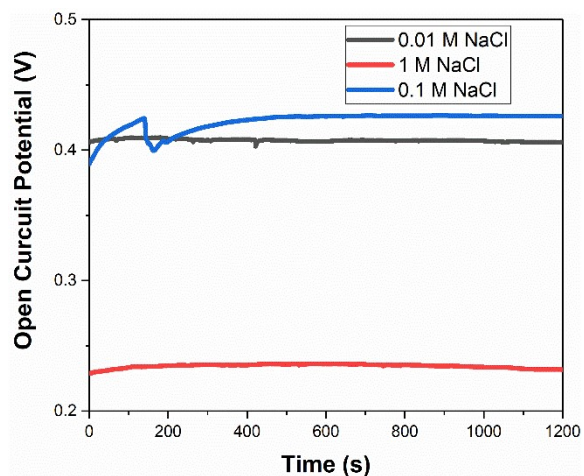
Figure S13. OCP plots of a 10-SILAR device in 0.01 M,0.1 M, and 1 M NaCl solutions.
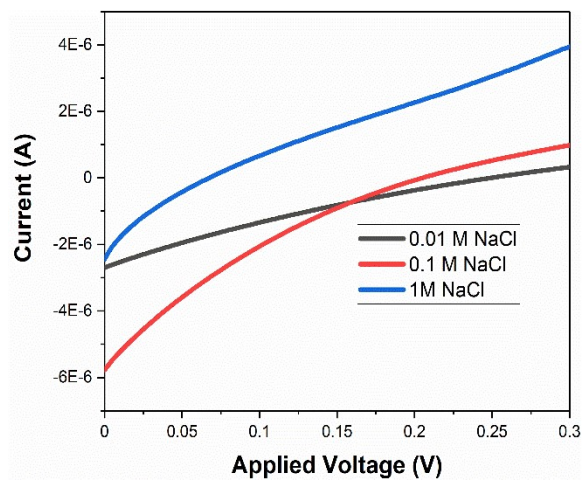
Figure S14. LSV plots of a 10-SILAR device in 0.01 M, 0.1 M, and 1 M NaCl solutions.

6. AuNP Leaching Study
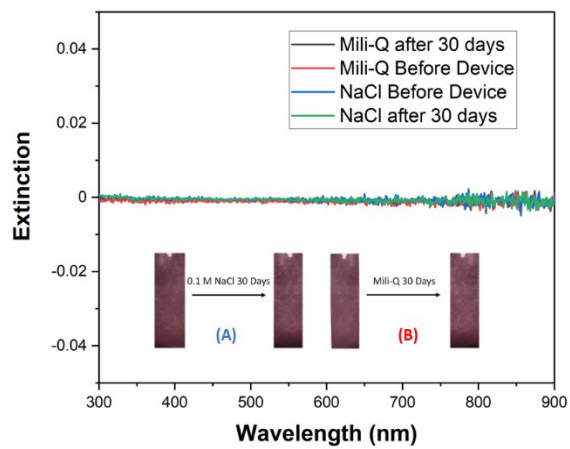
Figure S15. Device extinction (A) before and after 30 days in NaCl solution and (B) before and after 30 days in Mili-Q solution. Insets of the devices at day zero and day thirty are included on the plot.

7. AuNP Weight Percentage and Error Propagation

Table S1: Total mass of decorated filter paper and the mass contributions of AuNP for each device tested

Mass of Device (mg)	Mass of AuNP (mg)	SILAR Growth Cycles
48.66 ± 0.38	0 (Bare Filter Paper)	0
48.84 ± 0.40	0.18 ± 0.02	5
48.90 ± 0.42	**0.24** ± 0.04	**10**
49.01 ± 0.41	0.34 ± 0.03	20
49.08 ± 0.38	0.42 ± 0.04	40

7.1 AuNP Weight Percentage

The weight percent of the gold nanoparticles grown on each device was calculated using Equation 5:

$$wt\%_{AuNP} = \frac{m_{AuNP}}{m_{device}} \times 100\% \#(5)$$

Where: m_{AuNP} is the mass of gold nanoparticles grown on the filter paper devices, and m_{device} is the total mass of the device (filter paper mass plus gold nanoparticle mass).

This treatment was used for each device and a representative calculation for the best performing device (10-SILAR cycles) is shown below (m_{AuNP} = 0.24 mg V; m_{device} = 48.90 mg):

$$wt\%_{AuNP} = \frac{0.24 \, mg}{48.90 \, mg} \times 100\% = 0.49\%$$

7.2 AuNP Weight Percentage Error Propagation

The error in weight percentage for each device was calculated by propagating the standard deviation for each measurement using Equation 6:

$$\delta wt\%_{AuNP} = |wt\%_{AuNP}| \sqrt{\left(\frac{\delta m_{AuNP}}{m_{AuNP}}\right)^2 + \left(\frac{\delta m_{device}}{m_{device}}\right)^2} \#(6)$$

Where: $wt\%_{AuNP}$ is the weight percent of gold nanoparticles grown on the device, m_{AuNP} is the mass of gold nanoparticles grown on the filter paper devices, and m_{device} is the total mass of the device (filter paper mass plus gold nanoparticle mass). Further, $\delta wt\%_{AuNP}$, δm_{AuNP}, and δm_{device} denote the error in weight percentage, mass of gold nanoparticles, and mass device.

The error calculation remained the same for each device and so a representative calculation for the best performing device (10-SILAR cycles) is shown below:

$$\delta Pd = |0.49\%| \sqrt{\left(\frac{0.04 \, mg}{0.24 \, mg}\right)^2 + \left(\frac{0.42 \, mg}{48.9 \, mg}\right)^2} = \pm \, 0.08\%$$

8. Manufacturer and Reagent Purity

Reagents used in this work are listed with their manufacturer reported purity:

Sodium borohydride – Sigma (98%)

Chloroauric acid –Sigma Aldrich > 99.9% "Trace Metal Basis"

Sodium Chloride – Alfa Aesar (99.0%)

9. Power Generation from Different Hydrovoltaic Devices

To provide an appreciation for the power output density of gold-decorated filter paper devices, Table S2 highlights some additional materials reported in literature and their respective power output densities.

Table S2: Various reported hydrovoltaic materials and their respective power output density.

Materials	Power Output Density ($\mu W\ g^{-1}$)	References
Unprocessed Graphene Oxide Film	0.0023	[7]
Toluene Soot	0.172	[8]
Ni-Al LDH	0.18	[9]
Aluminum Oxide	1.026	[10]
Metal Organic Framework	3	[11]
Gold-Decorated Filter Paper	**3.3**	**This work**
Functionalized Carbon Nanotubes	210 (highest to date)	[12]

10. Sealed OCP measurement
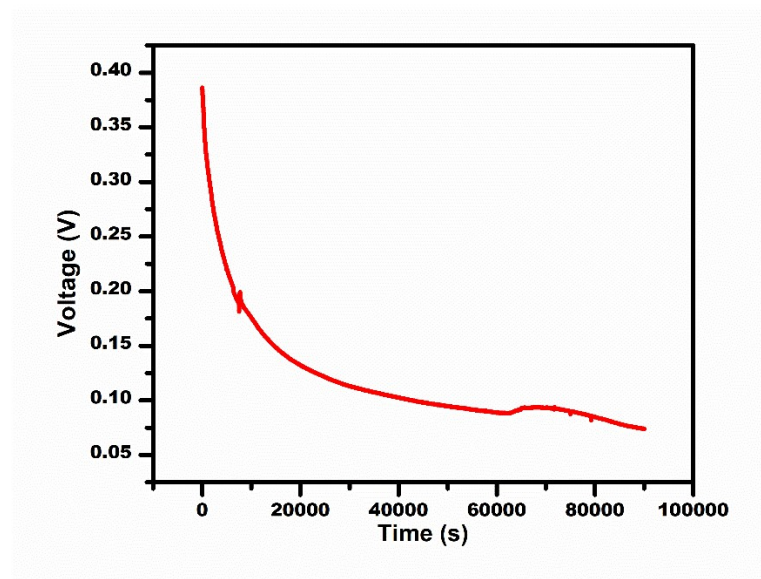
Figure S16. OCP vs Time for a 10 SILAR AuNP decorated filter paper device under fully sealed conditions

11. References

1. S. P. Ong, W. D. Richards, A. Jain, G. Hautier, M. Kocher, S. Cholia, D. Gunter, V. L. Chevrier, K. A. Persson and G. Ceder, *Computational Materials Science*, 2013, **68**, 314-319.
2. A. A. Bunaciu, E. g. Udriştioiu and H. Y. Aboul-Enein, *Critical Reviews in Analytical Chemistry*, 2015, **45**, 289-299.
3. S. Balasubramani and B. Kumari, *Journal of Trace Elements in Medicine and Biology*, 2017.
4. P. Mukherjee, C. R. Patra, A. Ghosh, R. Kumar and M. Sastry, *Chemistry of Materials*, 2002, **14**, 1678-1684.
5. J. I. Langford and A. J. C. Wilson, *Journal of Applied Crystallography*, 1978, **11**, 102-113.
6. Bruker, *D2 PHASER 2nd Generation: Diffraction Solutions*, 2017.
7. Y. Liang, F. Zhao, Z. Cheng, Y. Deng, Y. Xiao, H. Cheng, P. Zhang, Y. Huang, H. Shao and L. Qu, *Energy & Environmental Science*, 2018, **11**, 1730-1735.
8. T. Ding, K. Liu, J. Li, G. Xue, Q. Chen, L. Huang, B. Hu and J. Zhou, *Advanced Functional Materials*, 2017, **27**, 1700551.
9. J. Sun, P. Li, J. Qu, X. Lu, Y. Xie, F. Gao, Y. Li, M. Gang, Q. Feng, H. Liang, X. Xia, C. Li, S. Xu and J. Bian, *Nano Energy*, 2019, **57**, 269-278.
10. C. Shao, B. Ji, T. Xu, J. Gao, X. Gao, Y. Xiao, Y. Zhao, N. Chen, L. Jiang and L. Qu, *ACS Applied Materials & Interfaces*, 2019, **11**, 30927-30935.
11. Q. Ma, Q. He, P. Yin, H. Cheng, X. Cui, Q. Yun and H. Zhang, *Advanced Materials*, 2020, **32**, 2003720.
12. R. Kumar, T. Tabrizizadeh, S. Chaurasia, G. Liu and K. Stamplecoskie, *Sustainable Energy & Fuels*, 2022, **6**, 1141-1147.